

From Waste-Heat Recovery to Refrigeration: Compositional Tuning of Magnetocaloric Mn_{1+x}Sb

Joya A. Cooley,[†] Matthew Horton,[‡] Emily E. Levin,^{†,¶} Saul H. Lapidus,[§]

Kristin A. Persson,^{‡,||} and Ram Seshadri^{*,†,¶,⊥}

*[†]Materials Research Laboratory, University of California, Santa Barbara
California 93106, United States*

*[‡]Energy Storage and Distributed Resources Division, Lawrence Berkeley National Laboratory
Berkeley, California 94720, United States*

*[¶]Materials Department, University of California, Santa Barbara
California 93106, United States*

*[§]X-ray Sciences Division, Argonne National Laboratory
Lemont, Illinois 60439, United States*

*^{||}Materials Science and Engineering, University of California, Berkeley
California 94720, United States*

*[⊥]Department of Chemistry and Biochemistry, Santa Barbara
California 93106, United States*

E-mail: seshadri@mrl.ucsb.edu

Abstract

Magnetic refrigeration as well as waste-heat recovery can be accomplished through the magnetocaloric effect, where temperature gradients change the magnetic state of a material, or *vice versa*. Promising magnetocaloric materials display large changes in entropy upon application of a moderate magnetic field, quantified as the isothermal magnetic entropy change ΔS_M , often associated with magnetic materials possessing some degree of magnetostructural coupling. In such compounds, the magnetic transition is coupled to a first-order structural change at the ordering temperature, and indicators for these are readily calculated by the magnetic deformation proxy Σ_M . MnSb, with a Curie temperature $T_C = 577$ K is associated with a calculated magnetic deformation of $\Sigma_M = 5.9\%$, and is a promising candidate material for waste-heat recovery. The temperature-dependence of structure, magnetic, and magnetocaloric properties of Mn_{1+x}Sb , where x is a tunable amount of interstitial Mn are studied here. The inclusion of interstitial Mn has the effect of lowering T_C , such that the Curie temperature can be tuned from 577 K to nearly room temperature at 318 K for $x = 0.2$. For $x = 0.0$, 0.1, and 0.2, values of ΔS_M under a maximum magnetic field $H = 5$ T are found to be $3.65 \text{ JK}^{-1} \text{ kg}^{-1}$, $3.00 \text{ JK}^{-1} \text{ kg}^{-1}$, and $2.83 \text{ JK}^{-1} \text{ kg}^{-1}$, respectively. While the maximum ΔS_M decreases with x , the high refrigerant capacity — a more holistic measure of performance — is retained.

Introduction

Continued efforts to decrease energy use and recover waste heat has led to a focus on magnetocaloric materials, which are promising in applications ranging from refrigeration^{1,2} to waste-heat recovery.³ Key to these applications is the magnetocaloric effect (MCE) where a change in applied magnetic field induces a reversible change in temperature. With appropriate cycling, refrigeration becomes possible. This application has been studied and applied at cryogenic temperatures and at room temperature for refrigeration purposes.² The complementary process, termed the reverse MCE, is when a temperature gradient induces changes in the magnetic state. Inverse MCE can be harnessed into useful mechanical or electrical energy.² An important figure of merit governing the performance of magnetocaloric materials is the entropy change due to magnetization ΔS_M . Since ΔS_M is maximized near T_C , the ability to tune T_C , and thus the temperature at which a material is most effective, is valuable from an applications standpoint. Rare-earth free⁴ compounds and those not containing toxic elements⁵⁻⁹ are particularly appealing. Research in the last few decades has focused extensive efforts solid-state refrigeration devices using the Peltier effect as well as thermal energy harvesting technologies such as thermoelectrics using the Seebeck effect,¹⁰ pyroelectrics,^{11,12} thermoelastics,¹³ and thermomagnetism using the reverse magnetocaloric effect (MCE).¹⁴ A review comparing these different strategies has appeared recently.¹⁵ While the MCE has long been studied for refrigeration and cryogenic cooling, it has been proposed that the reverse MCE for the recovery of low grade heat is a viable option.³

In the search for useful magnetocaloric materials, We have employed a previously described computational proxy for the degree of magnetostructural coupling in a material, the magnetic deformation Σ_M which correlates well with ΔS_M .^{16,17} The results of these calculations show that MnSb may be a good magnetocaloric material as indicated by its calculated magnetic deformation, $\Sigma_M = 5.87\%$. This follows the trend suggested by binary compounds of transition metals and metalloids in the NiAs structure type, which show a

host of types of magnetic ordering and varying degrees of magnetostructural coupling. It is well known that this compound exists only as Mn_{1+x}Sb , where x indicates the amount of excess Mn hosted on an interstitial site. Under extreme conditions, x has been found to reach up to 0.5,¹⁸ but under more usual preparation conditions, x is between 0.02 and 0.25.¹⁹ Most pertinent to the present study, the amount of interstitial Mn greatly affects the structure and magnetism, and can be used to tune T_C in a predictable way. It has been proposed that the equation $T_C = (577 - 790 \times x)$ accounts for the behavior of T_C with respect to the amount of interstitial Mn, x , in the structure.^{19,20}

In this work, we present a study of the magnetocaloric performance of Mn_{1+x}Sb with nominal x values 0.0, 0.1, and 0.2. We are able to exhibit control T_C and, in turn, the temperature of the maximum $|\Delta S_M|$. While it is unlikely that T_C control is because of a simple unit cell volume change,²¹ we suggest the T_C decrease is due to increased magnetic disorder in the lattice, and density functional theory calculations suggest that the lowest-energy configurations correspond to the interstitial Mn moments antiparallel to the principal Mn moments. The magnitude of ΔS_M decreases as x increases, but we show that the refrigerant capacity, remains robust at all doping levels. Furthermore, we suggest that, while maximum ΔS_M decreases with increasing interstitial concentration, this is entirely predictable based on the decreasing Σ_M value, suggesting that the degree of magnetostructural coupling changes as as interstitial inclusion is increased. The high ΔS_M and T_C tunability make this series uniquely interesting for both magnetic refrigeration and waste-heat recovery applications.

Materials and Methods

Synthesis Polycrystalline powders of MnSb were prepared using a one-step solid state synthesis. Elemental Mn (99.95%, Alfa Aesar) was purified before synthesis by annealing overnight sealed in an evacuated fused silica tube at 1273 K. Purified Mn was then ground

and combined with Sb powder ground from shot (99.999%, Alfa Aesar) according to the targeted stoichiometry (e.g. $\text{Mn}_{1.1}\text{Sb}$ measured as 1.1 mole Mn and 1.0 mole Sb) to total masses of 0.50 g to 0.75 g. Pre-weighed Mn and Sb powders were combined, ground in an agate mortar and pestle, and pelletized into 6 mm pellets. Pellets were placed in boron nitride crucibles, sealed in evacuated fused silica ampoules, and annealed at 1123 K for 48 h before the furnace was turned off and allowed to cool. For clarity, samples will be referred to according to their nominal Mn compositions (i.e. $x = 0.0, 0.1,$ and 0.2).

Structural characterization High-resolution synchrotron powder X-ray diffraction (XRD) data were collected at room temperature on samples of Mn_{1-x}Sb , $x = 0, 0.1,$ and $0.2,$ and at several temperatures above and below T_C on $x = 0.0$ using beamline 11-BM at the Advanced Photon Source (APS), Argonne National Laboratory. For room temperature scans, powderized samples were loaded into a 0.8 mm diameter Kapton capillary and measured with $\lambda = 0.412801 \text{ \AA}$. For the high temperature measurements a 1.1 mm diameter fused silica capillary and sealed on each end with clay was used, and measured with $\lambda = 0.412825 \text{ \AA}$. During the multi-temperature measurement, temperature was swept at 0.5 K min^{-1} while collecting 10 min scans between $0.00 2\theta$ and $6.00 2\theta$ (Q approximately ranging from 0.13 \AA^{-1} to 7.35 \AA^{-1}), such that each scan encompasses approximately 5 K. Rietveld refinements of data were performed using TOPAS and structures visualized using VESTA-3.²²

Magnetic measurements Magnetic properties were measured on 5 mg to 15 mg pieces of annealed pellets in a Quantum Design MPMS3 SQUID vibrating sample magnetometer (VSM). Pieces of each sample were attached to the Quantum Design oven stick, capable of high temperature measurements, with Zircar cement, and cured with a heat gun for 30 s to 1 min. Because of the lower T_C of $x = 0.2,$ this sample was measured in a VSM powder sample holder using chamber temperature control. Zero field- and field-cooled magnetization (M) vs temperature (T) measurements were taken upon warming at a

rate of 7 K min^{-1} . Arrott plots were constructed with one quadrant of M vs applied field (H) measurements (i.e., 0 T to 5 T) at 3 K intervals above and below the approximate T_C ; details for each composition can be found in the Supporting Information. In order to determine ΔS_M , M versus T measurements were taken on cooling (using a rate of 5 K min^{-1}) at various fields from $H = 0.1 \text{ T}$ to $H = 5 \text{ T}$. Further details of ΔS_M calculations have been reported elsewhere.²³

Electronic structure calculations Previous work established Σ_M as a descriptor for magnetocaloric materials, whereby a structural relaxation was performed within conventional density functional theory (DFT) for a given crystal structure initialized in both a ferromagnetic order and also in non-spin-polarized configuration where magnetic moments are constrained to be zero. This latter case, though an idealized configuration and not directly comparable to a paramagnetic state, is sufficient to capture a measure of magnetostructural coupling through a comparison of the equilibrium lattice parameters in both cases, and this was found to correlate well to ΔS_M . A high-throughput screening of inorganic materials sourced from the Materials Project²⁴ revealed that MnSb was one such material with a Σ_M of 5.87% significantly higher than the 1.5% cut-off proposed for promising magnetocalorics.¹⁶

All DFT calculations were performed using the Vienna Ab initio Simulation Package²⁵ and using standard settings suggested by the ATOMATE²⁶ software package and also its workflows for magnetic materials,²⁷ including projector augmented wave pseudopotentials with Mn including 3p, 3d and 4s electrons as valence, a plane-wave cut-off of 520 eV, and a k -point density of at least $64 \text{ } k\text{-points } \text{\AA}^{-3}$. For calculation of magnetic deformations, two approaches were attempted. The first in which all Mn atoms were initialized in a ferromagnetic configuration, and another where the host Mn atoms were initialized in a ferromagnetic configuration but the Mn interstitial atoms initialized with anti-parallel spin for an overall ferrimagnetic ordering. While both configurations produced qualiti-

tively similar trends, the results reported here are for the more physical and lower-energy ferrimagnetic orderings.

The DFT method cannot simulate disordered cells so ordered approximations were constructed for the intermediate compositions containing interstitial Mn using the PYMATGEN²⁸ package. For each composition, three separate ordered approximations were taken with cells containing approximately fifty atoms, and the magnetic deformation calculated for each and their means reported. For each composition, the difference in magnetic deformation between different ordered approximations was low, with 4.21 %, 4.49 % and 4.75 % for $x = 0.1$ and 3.68 %, 3.74 % and 3.78 % for $x = 0.2$, so this approximation was considered sufficient for establishing the expected trends in magnetic deformation as interstitial content was increased.

Results and discussion

Structural characterization

The unit cell of MnSb in the NiAs structure type is pictured in Figure 1(a), with the pseudo-octahedral coordination environment of Mn ($2a$ site) emphasized. Figure 1(b) depicts the same view of the unit cell, but with the trigonal bipyramidal coordination of the partially occupied interstitial Mn position ($2d$ site) emphasized. It is worth noting that the partial occupation of the Mn_i position results in the Ni_2In structure type. We employ the Kröger-Vink notation and refer to the stoichiometric Mn position as Mn_{Mn} and interstitial position as Mn_i .²⁹

Figure 2(a) shows a representative Rietveld refinement of synchrotron X-ray diffraction data for $x = 0.2$. Full diffraction patterns and decompositions for each sample can be found in the Supporting Information. In each sample, the major phase is MnSb, yet there is some degree of sample inhomogeneity. A second MnSb phase with a slightly larger unit cell volume, suggesting a slightly higher Mn_i content, can be fit to the pattern, and this has

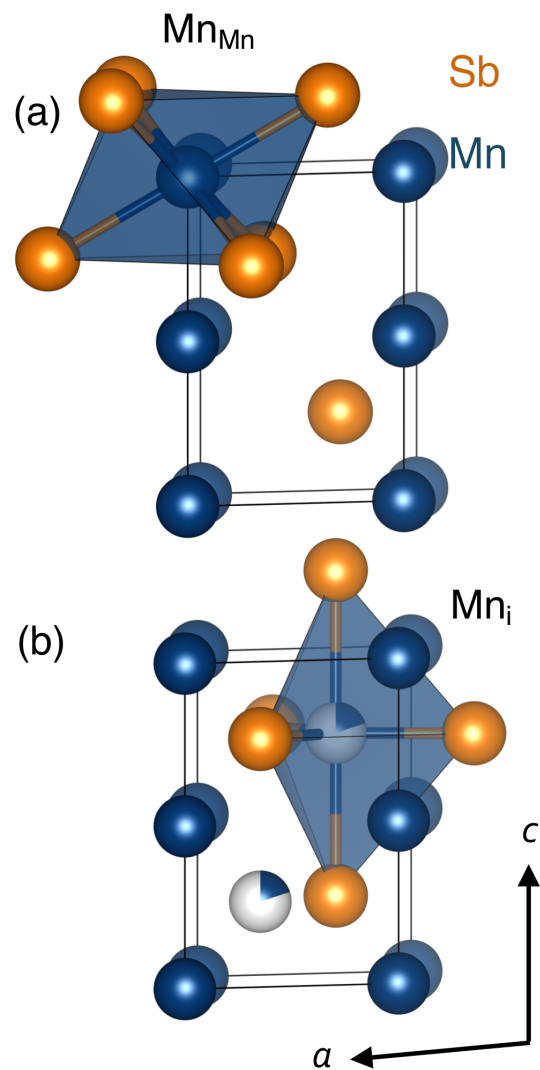


Figure 1: (a) One unit cell of stoichiometric MnSb is depicted with the octahedral coordination of the Mn_{Mn} site emphasized. (b) The unit cell is shown including the coordination of partially occupied Mn_i site with trigonal bipyramidal coordination.

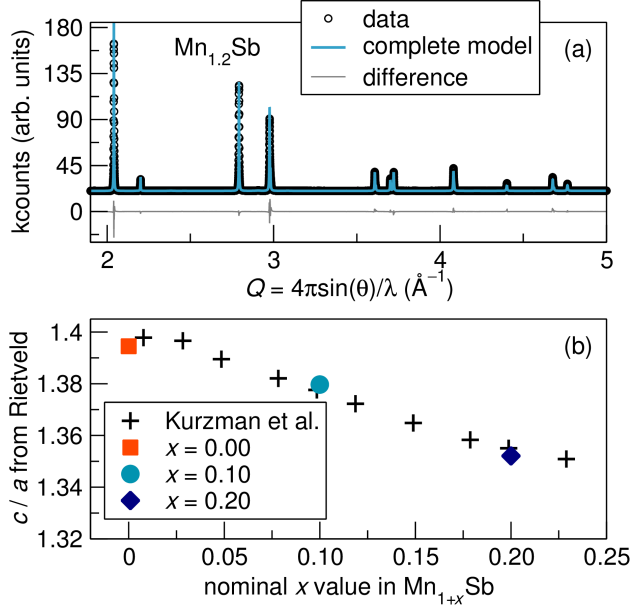


Figure 2: (a) Room-temperature synchrotron X-ray diffraction data fit to the hexagonal MnSb structure and the tetragonal Mn_2Sb structure (2.4 wt%). (b) c/a ratio as determined by Rietveld refinement of X-ray diffraction data (closed symbols) compared to literature values (plus signs, from Kurzman *et al.*²⁹) showing a decreasing trend.

previously been shown to occur in CrTe which is also in the NiAs structure type.³⁰ Because of the degree of peak overlap between these phases, an approximate Mn_i composition as determined by Rietveld refinement is unreliable, but this did not interfere with reliable determination of unit cell parameters of the main phase. Several other methods of confirming increasing interstitial inclusion are discussed below. The stoichiometric $x = 0$ compound has proven difficult to synthesized precisely, and measurements on single-crystals show some degree of interstitial composition, even when the stoichiometric phase is targeted.¹⁹

In addition, $x = 0.0$ contains a small amount ($<1\%$) of elemental Sb , however this should have no effect on measured magnetic properties and magnetocaloric performance as Sb is magnetically silent. $x = 0.2$ is near the Mn solubility limit and shows formation of Mn_2Sb ($P4/nmm$, No. 129), a ferrimagnet found to order near 550 K,³¹ and the formation of this impurity is also seen in single crystal growth.³² Although this particular impurity phase is magnetic, its high ordering temperature as compared to $x = 0.2$ (discussed later) implies it should have a negligible, if any, effect on the magnetocaloric performance of

$x = 0.2$.

As previously discussed, occupation of the Mn_i position increases the a lattice parameter while decreasing the c lattice parameter, resulting in an overall increase in unit cell volume and decrease in the c/a ratio. Kurzman *et al.* systematically studied the c/a ratio decrease as a function of nominal composition through refinement of both high-resolution synchrotron powder diffraction and pair distribution function measurements, which were in excellent agreement with one another.²⁹ In Figure 2(b), the c/a ratios derived from Rietveld refinement of synchrotron data (closed symbols) are compared to the Kurzman data (open symbols) and show excellent agreement. These data are thus a good indicator that the Mn_i position is increasingly being occupied.

Temperature-dependent structure

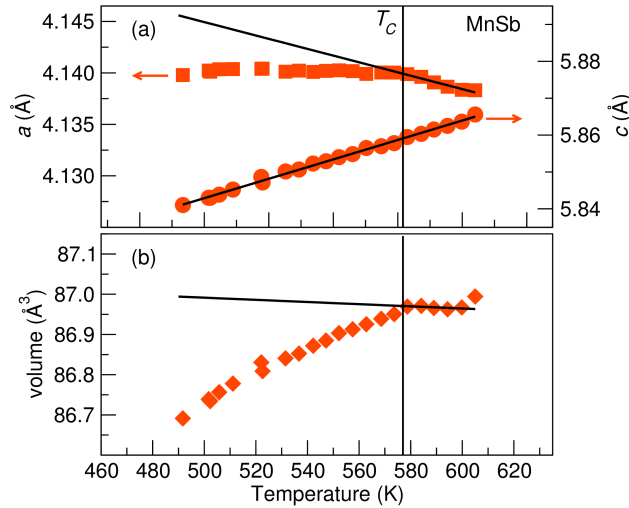


Figure 3: Temperature-dependent lattice parameters a and c derived from Rietveld refinement of temperature-dependent synchrotron X-ray diffraction data on $x = 0.0$. In both panels, the solid vertical line is the approximate T_C , and the sloped lines indicate the best linear fit to paramagnetic (i.e. above T_C) unit cell parameter data above T_C .

Figure 3 shows the dependence of the unit cell parameters (a) a and c as well as (b) the unit cell volume (as determined by Rietveld refinement) on temperature as heated through T_C in $x = 0.0$. It is clear that the temperature dependence of the c parameter does

not change significantly throughout the temperature range measured here. However, the a parameter exhibits negative thermal expansion (NTE) above T_C , then shows a noticeable shift in slope near 575 K, very near to T_C . Below T_C , the temperature dependence resembles an Invar effect, where thermal expansion becomes invariant below T_C ,³³ but is only observed in the a direction. The shift in slope is also quite prominent in the temperature dependent unit cell volume, where above T_C the slope is -2.69×10^{-4} and shifts to 3.1×10^{-3} below T_C . As was predicted by the magnitude of Σ_M , we clearly observe a change in the coefficient of thermal expansion manifesting itself as negative spontaneous volume magnetostriction (ω_V) near the expected T_C . ω_V can be quantified according to the following equation:^{34,35}

$$\omega_V(T) = \frac{(V - V_p)}{V_p} \quad (1)$$

where V is the experimental value of the unit cell volume at a temperature, T , and V_p is unit cell volume calculated from extrapolating the temperature dependence in the paramagnetic state (above T_C) to temperature T . For $x = 0$, $\omega_V = -0.003$ at 490 K, which clearly confirms a negative spontaneous volume magnetostriction. Many Mn-based magnets show positive spontaneous volume magnetostriction at the Curie or Neèl temperature, such as LaMnO_3 ,³⁶ MnAs ,³⁷ YMn_2 ³⁸ as well as several Mn-based compounds in the Ni_2In structure type.³⁹ However negative volume magnetostriction is not unprecedented in Mn-based materials and both MnO and MnS exhibit it at their Neèl temperatures.⁴⁰

The overall results are in agreement with the original reports on this material which also show the dependence of c to be uniform between 300 K and 770 K, but show a discontinuity in the a direction near T_C .⁴¹ The previous results also suggest that the anomalous thermal expansion below T_C (manifesting as NTE in the present work) resembles a type of electronic NTE mechanism. Through this mechanism, on either side of the phase transition, the material exhibits conventional positive thermal expansion (PTE), but in some region where there is crossover between two phases (e.g., a non-magnetic and magnetic

phase), NTE occurs.⁴² While the results of Willis *et al.* are in good agreement with this mechanism, the results of the present work are somewhat inconsistent with this mechanism. In this work, NTE actually occurs before the expected paramagnetic-to-ferrimagnetic phase transition, in the region where phase-crossover is not necessarily expected. Additionally, Willis *et al.* show that the thermal expansion anomaly appears more like near-zero thermal expansion (NZTE) in the crossover region, and is sustained over nearly 100 K, however the data density is low (4 data points over a 100 K range). The precise details, and perhaps elucidation of the mechanism driving the thermal expansion anomaly, could be better understood by acquiring temperature-dependent high-resolution synchrotron X-ray diffraction data at higher temperatures, perhaps above the suggested crossover region, with higher data density.

Magnetic characterization

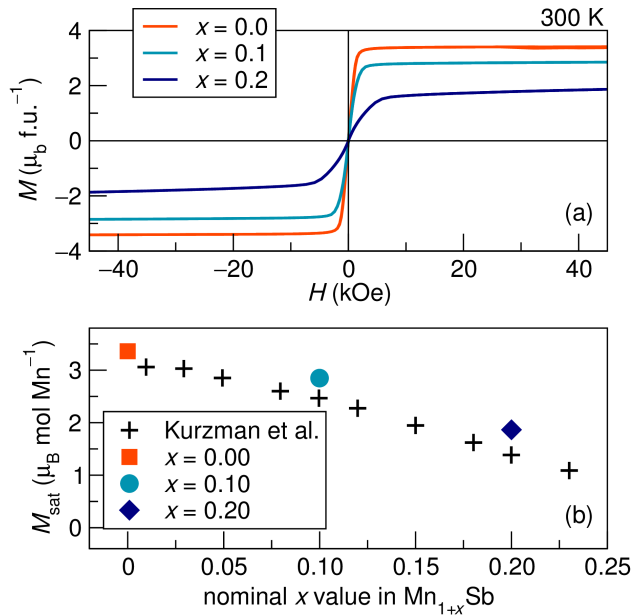


Figure 4: (a) Field-dependent magnetization data at 300 K for $x = 0.0, 0.1,$ and 0.2 showing a decreasing trend in saturation magnetization. (b) M_{sat} data from field-dependent magnetization measurements for data presented in this work (closed symbols) and previous literature (plus signs, from Kurzman *et al.*²⁹)

Magnetic properties of Mn_{1+x}Sb have long been studied, but recently Taylor *et al.* set-

led an important debate on whether or not the Mn_i possesses a magnetic moment.²¹ It has been seen that the inclusion of Mn_i decreases the saturation magnetization, M_{sat} , which can be explained by an antiparallel moment on Mn_i . As previously discussed, the antiparallel orientation of the Mn_i moment with respect to that of Mn_{Mn} is expected to decrease the overall M_{sat} as Mn_i composition increases. Figure 4(a) depicts field-dependent magnetization traces (M vs H) measured at room temperature. Each shows magnetic ordering at relatively low field, and as the nominal excess Mn increases the curve saturates at lower values. In Figure 4(b), a comparison between M_{sat} values vs H for the data measured by Kurzman et al. (plus signs) and present samples (closed symbols) are shown to be in good agreement, further validating increasing interstitial inclusion.

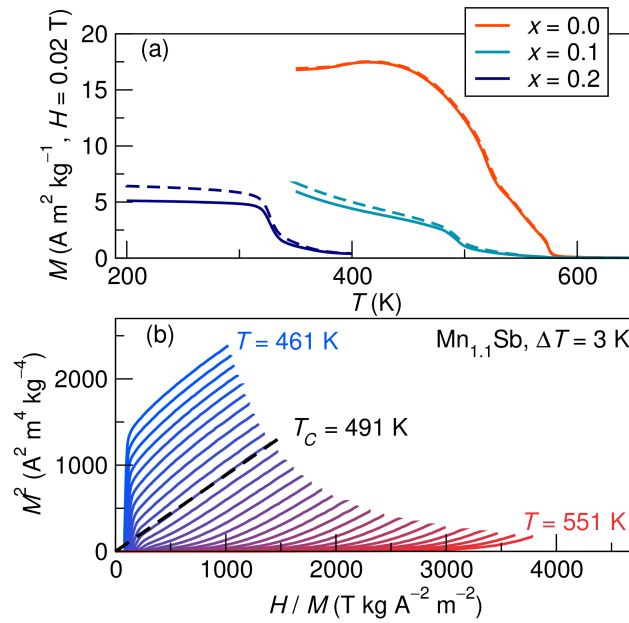


Figure 5: (a) Zero-field-cooled (solid) and field-cooled (dashed) temperature-dependent magnetization data measured using $H = 200\ Oe$ for $x = 0.0, 0.1,$ and 0.2 . (b) Isothermal field-dependent magnetization scans plotted in the Arrott style for $x = 0.1$ yields $T_C \approx 491\ K$ (predicted as $498\ K$ from $T_C = (577 - 790 \times x)$).

Increasing interstitial inclusion increases T_C , and Figure 5(a) shows M vs T traces for each sample measured with $H = 200\ Oe$. Each sample shows little thermomagnetic irreversibility, consistent with their low coercive fields (H_C) at room temperature. Additionally, the transitions from the paramagnetic to ferrimagnetic states clearly at decreasing

temperatures with increasing Mn_i composition. While this fits the expected trend, the precise ordering temperatures are difficult to assign due to the broadness of the transitions (likely due to the aforementioned sample inhomogeneity). To assign more precise ordering temperatures, several isothermal M vs H traces were measured for each sample through each approximate T_C . When these data are plotted in the Arrott format (M^2 vs H/M),⁴³ the isotherm that extrapolates to the origin indicates T_C . Figure 5(b) shows the Arrott plot representative example, $x = 0.1$, where T_C is found to be 491 K, which is in good agreement with the experimental T_C calculated using $T_C = (577 - 790 \times x, 498 \text{ K})$. The agreement is similar for $x = 0.0$ where the experimental T_C is determined to be 560 K and the calculated T_C is 577 K (Figure S5 of the Supporting Information). There is a much larger discrepancy between the experimentally determined (339 K) and calculated (419 K) T_C values for $x = 0.2$ (Figure S6 of the Supporting Information) that is as yet unexplained and will require further investigation.

Magnetocaloric performance

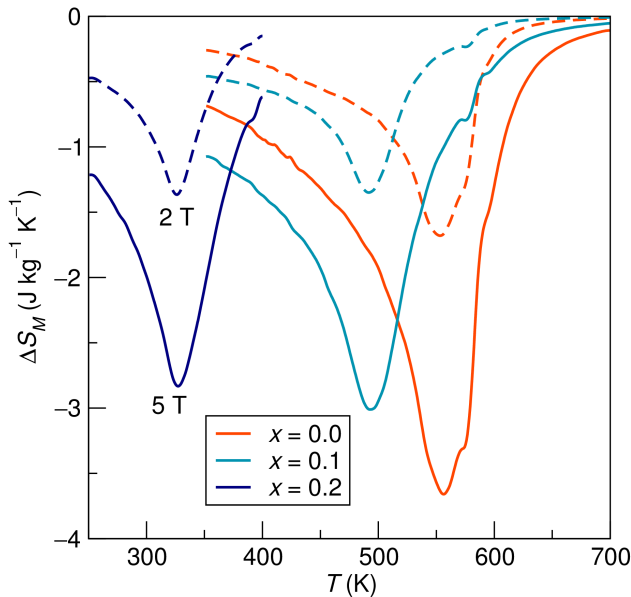


Figure 6: Calculated ΔS_M traces for $x = 0.0, 0.1,$ and 0.2 for select field changes.

In order to calculate ΔS_M , temperature-dependent magnetization was measured

through T_C at varying fields, derived, and integrated over field to produce the ΔS_M traces shown in Figure 6; the complete sets of M vs. T data, derivative traces, and ΔS_M traces for each composition can be found in the Supporting Information. It is clear from the peak of each ΔS_M curve that the T_C , and therefore temperature of maximum magnetocaloric effect decreases as Mn interstitial inclusion increases.

It is also of note that the maximum value of ΔS_M decreases slightly as interstitial inclusion increases. Here, we make two comments about the decreasing magnetocaloric performance, the first being that this decrease is not unexpected based on the computational results. Figure 7(c) and (d) show the computationally derived Σ_M parameter for each composition and experimentally determined maximum $|\Delta S_M|$, respectively, for each composition. It is suggested by the decreasing Σ_M values that the degree of magnetostructural coupling decreases as the interstitial is added in such a way that the magnetoelastic transition is somehow lessened, and this is corroborated by the decreasing absolute value of ΔS_M .

The second point is that the refrigerant capacity, discussed in the introduction, remains relatively robust, especially between the nominally stoichiometric and $x = 0.1$ samples. Refrigerant capacity was first introduced by Wood et al.⁴⁴ and further developed by Gschneider et al.¹ as a measure of the heat transferred between sides in one refrigeration cycle. Refrigerant capacity (RC) can be calculated as

$$RC = \int_{T_{cold}}^{T_{hot}} \Delta S(T, P, \Delta H)_{P, \Delta H} dT \quad (2)$$

Figures 7(a)–(e) show magnetic and magnetocaloric properties for each sample, including the calculated RC value. The case of RC remaining robust is nicely illustrated in that there is a very clear decrease in the maximum ΔS_M from $x = 0.0$ to 0.1 seen in Figure 6. Qualitatively, while the $x = 0.1$ ΔS_M peak is not as sharp, its FWHM is over a broader temperature range, meaning that although the maximum ΔS_M has decreased, the RC remains nearly the same, and actually slightly increases. This indicates the overall

performance may not be affected much just based on the simple decrease in maximum ΔS_M . The RC value for the $x = 0.2$ sample RC is also still in line with other materials with similar or higher ΔS_M values for the same field change.²

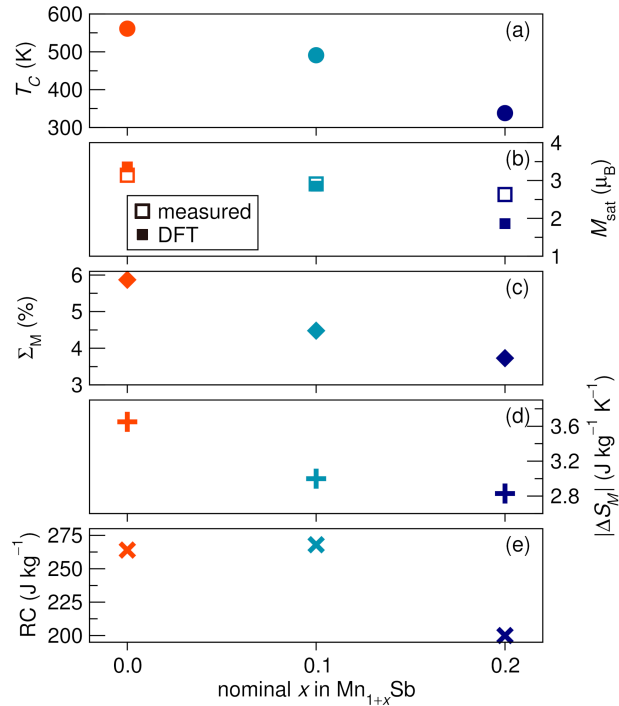


Figure 7: A summary of magnetic and magnetocaloric properties of each sample vs its nominal x value is shown including (a) T_C from Arrott analysis, (b) the DFT (open symbols) and measured (closed symbols) M_{sat} , (c) the computed Σ_M , (d) the experimentally determined $|\Delta S_M|$, and (e) the refrigerant capacity.

Conclusion

In closing T_C can be tuned from high temperatures (561 K) to nearly room temperature (318 K) using interstitial composition (x in $Mn_{1+x}Sb$) as a tuning parameter. The change in magnitude of ΔS_M with changing x follows the trend suggested using the DFT-based magnetic deformation proxy Σ_M . Although tuning T_C down to room temperature causes a decrease in the maximum ΔS_M , the refrigerant capacity throughout the series remains robust, suggesting that overall magnetocaloric performance would not be impacted much

by x inclusion. Furthermore, the prediction of decreasing ΔS_M with increasing x indicates that there is a change in the degree of magnetostructural coupling as the interstitial concentration increases and this may be worthy of further investigation.

Acknowledgements

This work was supported by the National Science Foundation through DMR-SSMC 1710638. The research reported here made use of shared experimental facilities of the National Science Foundation (NSF) Materials Research Science and Engineering Center at UC Santa Barbara (DMR 1720256). The UCSB MRSEC is a member of the Materials Research Facilities Network (www.mrnf.org). Use of the Advanced Photon Source at Argonne National Laboratory was supported by the U. S. Department of Energy, Office of Science, Office of Basic Energy Sciences, under Contract No. DE-AC02-06CH11357. KAP and RS would like to acknowledge BASF for initial support of research into magnetocalorics.

References

- (1) Pecharsky, V. K.; Gschneider, Jr., K. A. Some Common Misconceptions Concerning Magnetic Refrigerant Materials. *J. Appl. Phys.* **2001**, *90*, 4614–4622.
- (2) Franco, V.; Blázquez, J.; Ingale, B.; Conde, A. The Magnetocaloric Effect and Magnetic Refrigeration Near Room Temperature: Materials and Models. *Annu. Rev. Mater. Res.* **2012**, *42*, 305–342.
- (3) Kishore, R. A.; Priya, S. Low-Grade Waste Heat Recovery Using the Reverse Magnetocaloric Effect. *Sustainable Energy Fuels* **2017**, *01*, 1–10.
- (4) Brück, E.; Tegus, O.; Thanh, D. T. C.; Trung, N. T.; Buschow, K. H. J. A Review on Mn

- Based Materials for Magnetic Refrigeration: Structure and Properties. *Int. J. Refrig.* **2008**, *31*, 763–770.
- (5) Tan, X.; Chai, P.; Thompson, C. M.; Shatruk, M. Magnetocaloric Effect in AlFe_2B_2 : Toward Magnetic Refrigerants from Earth-Abundant Elements. *J. Am. Chem. Soc.* **2013**, *135*, 9553–9557.
- (6) Ren, Q.; Hutchison, W. D.; Wang, J.; Studer, A. J.; Campbell, S. J. Magnetic and Structural Transitions Tuned through Valence Electron Concentration in Magnetocaloric $\text{Mn}(\text{Co}_{1-x}\text{Ni}_x\text{Ge})$. *Chem. Mater.* **2018**, *30*, 1324–1334.
- (7) Hering, P.; Friese, K.; Voigt, J.; Persson, J.; Aliouane, N.; Grzechnik, A.; Senyshyn, A.; Brückel, T. Structure, Magnetism, and the Magnetocaloric Effect of MnFe_4Si_3 Single Crystals and Powder Samples. *Chem. Mater.* **2015**, *27*, 7128–7136.
- (8) Boeije, M. F. J.; Roy, P.; Guillou, F.; Yibole, H.; Miao, X. F.; Caron, L.; Banerjee, D.; van Dijk, N. H.; de Groot, R. A.; Brück, E. Efficient Room-Temperature Cooling with Magnets. *Chem. Mater.* **2016**, *28*, 4901–4905.
- (9) Liu, J.; Gottschall, T.; Skokov, K. P.; Moore, J. D.; Gutfleisch, O. Giant Magnetocaloric Effect Driven by Structural Transitions. *Nat. Mater.* **2012**, *11*, 620–626.
- (10) Zhang, X.; Zhao, L.-D. Thermoelectric Materials: Energy Conversion Between Heat and Electricity. *J. Materiomics* **2015**, *1*, 92–105.
- (11) Lang, S. B. Pyroelectricity: From Ancient Curiosity to Modern Imaging Tool. *Phys. Today.* **2005**, *58*, 31–36.
- (12) Hunter, S. R.; Lavrik, N. V.; Mostafa, S.; Rajic, S.; Datskos, P. G. Review of Pyroelectric Thermal Energy Harvesting and New MEMs-Based Resonant Energy Conversion Techniques. *Proc. SPIE* **2012**, 8377.

- (13) Zhu, J. J.; Liang, N. G.; Liew, K. M.; Huang, W. M. Energy Conversion in Shape Memory Alloy Heat Engine Part I: Theory. *J. Intell. Mater. Syst. Struct.* **2001**, *12*, 127–132.
- (14) Kishore, R. A.; Priya, S. A Review on Design and Performance of Thermomagnetic Devices. *Renewable Sustainable Energy Rev.* **2018**, *81*, 33–44.
- (15) Kishore, R. A.; Priya, S. A Review on Low-Grade Thermal Energy Harvesting: Materials, Methods and Devices. *Materials* **2018**, *11*.
- (16) Bocarsly, J. D.; Levin, E. E.; Garcia, C. A. C.; Schwennicke, K.; Wilson, S. D.; Seshadri, R. A Simple Computational Proxy for Screening Magnetocaloric Compounds. *Chem. Mater.* **2017**, *29*, 1613–1622.
- (17) Bocarsly, J. D.; Levin, E. E.; Humphrey, S. A.; Faske, T.; Donner, W.; Wilson, S. D.; Seshadri, R. Magnetostructural Coupling Drives Magnetocaloric Behavior: The Case of MnB versus FeB. *Chem. Mater.* **2019**, *31*, 4873–4881.
- (18) Ryzhkovskii, V. M.; Goncharov, V. S. Effect of High-Pressure High-Temperature Processing on the Phase Composition and Magnetic State of Mn_{1+x}Sb ($0 \leq x \leq 1.0$) Alloys. *Inorg. Mater.* **2010**, *46*, 226–231.
- (19) Okita, T.; Makino, Y. Crystal Magnetic Anisotropy and Magnetization of MnSb. *J. Phys. Soc. Jpn.* **1968**, *25*, 120–124.
- (20) Yamaguchi, Y.; Watanabe, H.; Suzuki, T. Magnetic Moment of Excess Mn in $\text{Mn}_{1+\delta}\text{Sb}$. *J. Phys. Soc. Jpn.* **1976**, *41*, 703–704.
- (21) Taylor, A. E.; Berlijn, T.; Hahn, S. E.; May, A. F.; Williams, T. J.; Poudel, L.; Calder, S.; Fishman, R. S.; Stone, M. B.; Aczel, A. A.; Cao, H. B.; Lumsden, M. D.; Christianson, A. D. Influence of Interstitial Mn on Magnetism in the Room-Temperature Ferromagnet $\text{Mn}_{1+\delta}\text{Sb}$. *Phys. Rev. B* **2015**, *91*, 224418.

- (22) Momma, K.; Izumi, F. VESTA 3 for Three-Dimensional Visualization of Crystal, Volumetric and Morphology Data. *J. Appl. Cryst.* **2011**, *44*, 1272–1276.
- (23) Bocarsly, J. D.; Need, R. F.; Seshadri, R.; Wilson, S. D. Magnetoentropic Signatures of Skyrmionic Phase Behavior in FeGe. *Phys. Rev. B* **2018**, *97*, 100404.
- (24) Jain, A.; Montoya, J.; Dwaraknath, S.; Zimmermann, N. E. R.; Dagdelen, J.; Horton, M.; Huck, P.; Winston, D.; Cholia, S.; Ong, S. P.; Persson, K. In *Handbook of Materials Modeling : Methods: Theory and Modeling*; Andreoni, W., Yip, S., Eds.; Springer International Publishing: Cham, 2018; pp 1–34.
- (25) Kresse, G.; Furthmüller, J. Efficient Iterative Schemes for *ab initio* Total-Energy Calculations Using a Plane-Wave Basis Set. *Phys. Rev. B* **1996**, *54*, 11169–11186.
- (26) Mathew, K. et al. Atomate: A High-Level Interface to Generate, Execute, and Analyze Computational Materials Science Workflows. *Comput. Mater. Sci.* **2017**, *139*, 140–152.
- (27) Horton, M. K.; Montoya, J. H.; Liu, M.; A., P. K. High-Throughput Prediction of the Ground-State Collinear Magnetic Order of Inorganic Materials Using Density Functional Theory. *npj Comput. Mater.* **2019**, *5*.
- (28) Ong, S. P.; Richards, W. D.; Jain, A.; Hautier, G.; Kocher, M.; Cholia, S.; Gunter, D.; Chevrier, V. L.; Persson, K. A.; Ceder, G. Python Materials Genomics (pymatgen): A Robust, Open-Source Python Library for Materials Analysis. *Comput. Mater. Sci.* **2013**, *68*, 314–319.
- (29) Kurzman, J. A.; Martinolich, A. J.; Neilson, J. R. Influence of Interstitial Mn on Local Structure and Magnetism in $\text{Mn}_{1+\delta}\text{Sb}$. *Phys. Rev. B: Condens. Matter Mater. Phys.* **2015**, *92*, 1–10.

- (30) Gordienko, V. A.; Zubenko, V. V.; Nikolaev, V. I. Spontaneous Magnetostriction of CrTe. *J. Exp. Theor. Phys.* **1970**, *30*, 864–865.
- (31) Anand, K.; Christopher, N.; Kumar, J.; Gupta, A.; Singh, N. Coercivity Enhancement and Magnetic Property Evaluation of Bi Doped Mn₂Sb. *J. Magn. Magn. Mater.* **2019**, *476*, 29–34.
- (32) Chen, T.; Charlan, G. B.; Keezer, R. C. Growth of MnSb Single Crystals by Pulling With a Seed from Nonstoichiometric Molten Solution. *J. Cryst. Growth* **1977**, *37*, 29–36.
- (33) Nakamura, Y. The Invar Problem. *IEEE Trans. on Magn.* **1976**, *12*, 278–291.
- (34) Kusz, J.; Juszczak, S.; Warczewski, J. An X-ray Diffraction Study of Magnetostriction in Zn_{1-x}Cu_xCr₂Se₄ (0.2 < x < 1.0). *J. Appl. Crystallogr.* **1988**, *21*, 898–901.
- (35) Bombik, A.; Böhm, H.; Kusz, J.; Pacyna, A. W. Spontaneous Magnetostriction and Thermal Expansibility of TmFeO₃ and LuFeO₃ Rare Earth Orthoferrites. *J. Magn. Magn. Mater.* **2001**, *234*, 443–453.
- (36) Kadomtseva, A. M.; Popov, Y. F.; Vorob'ev, G. P.; Kamilov, K. I.; Ivanov, V. Y.; Mukhin, A. A.; Balbashov, A. M. Thermal-Expansion and Magnetostriction Anomalies in Phase Transitions in La_{1-x}Sr_xMnO₃. *Phys. Solid State* **2000**, *42*, 1110–1115.
- (37) Chernenko, V. A.; Wee, L.; McCormick, P. G.; Street, R. Giant Magnetoelastic Response in MnAs. *J. Appl. Phys.* **1999**, *85*, 7833–7837.
- (38) Shiga, M.; Wada, H.; Nakamura, Y. Magnetism and Thermal Expansion Anomaly of RMn₂ (R=Y, Gd, Tb, Ho and Er). *J. Magn. Magn. Mater.* **1983**, *31-34*, 119–120.
- (39) Hu, F.; Shen, F.; Hao, J.; Liu, Y.; Wang, J.; Sun, J.; Shen, B. Negative Thermal Expansion in the Materials With Giant Magnetocaloric Effect. *Front. Chem.* **2018**, *6*, 438.

- (40) Morosin, B. Exchange Striction Effects in MnO and MnS. *Phys. Rev. B* **1970**, *1*, 236–243.
- (41) Willis, B. T. M.; Rooksby, H. P. Magnetic Transitions and Structural Changes in Hexagonal Manganese Compounds. *Proc. Phys. Soc. B* **1954**, *67*, 290–296.
- (42) Attfield, J. P. Mechanisms and Materials for NTE. *Front. Chem.* **2018**, *6*, 371.
- (43) Arrott, A. Criterion for Ferromagnetism from Observations of Magnetic Isotherms. *Phys. Rev.* **1957**, *108*, 1394–1396.
- (44) Wood, M. E.; Potter, W. H. General Analysis of Magnetic Refrigeration and its Optimization Using a New Concept: Maximization of Refrigerant Capacity. *Cryogenics* **1985**, *25*, 667–683.